JMEPEG (2017) 26:1830–1838
DOI: 10.1007/s11665-017-2579-9

1059-9495/$19.00

Influence of Plastic Deformation on Martensitic Transformation During Hot Stamping of Complex Structure Auto Parts

Yuhan Shen, Yanli Song, Lin Hua, and Jue Lu

(Submitted September 6, 2016; in revised form December 23, 2016; published online February 27, 2017)

The ultra-high strength steel auto parts manufactured by hot stamping are widely applied for weight reduction and safety improvement. During the hot stamping process, hot forming and quenching are performed in one step wherein plastic deformation and phase transformation simultaneously take place and affect each other. Thereinto, the influence of deformation on martensitic transformation is of great importance. In the present paper, the influence of plastic deformation on martensitic transformation during hot stamping of complex structure auto parts was investigated. For this purpose, a B-pillar reinforced panel in B1500HS steel was manufactured by hot stamping, and the process was simulated by finite element software based on a thermo-mechanical-metallurgical coupled model. Considering various deformation degrees, the microstructures and mechanical properties at four typical locations of the hot stamped B-pillar reinforced panel were detected. The results show that the martensitic content and the microhardness increase with the increase in the deformation amount. There are two reasons causing this phenomenon: (1) the increase in mechanical driving force and (2) the increased probability of the martensitic nucleation at crystal defects. The x-ray diffraction analysis indicates the carbon enrichment in retained austenite which results from the carbon diffusion during the low-carbon martensite formation. Furthermore, the carbon content decreases with the increase in the deformation amount, because the deformation of austenite suppresses the carbon diffusion.

Keywords hot stamping, martensitic transformation, microstructures, microhardness, plastic deformation

1. Introduction

The development tendency of automobiles in future is energy-saving, consumption reduction and safety improvement. The application of UHSS in manufacturing automotive parts can not only achieve energy efficiency and emission reduction by reducing body weight, but also improve crashworthiness and security. At present hot stamping of UHSS sheets has been successfully used to produce automotive safety-related parts such as side impact beams, bumper beams, A-pillars and B-pillars (Ref 1). During hot stamping, the blank is initially heated up to an austenitizing temperature, and then non-isothermally formed and simultaneously quenched in the water-cooled press tools for martensitic transformation (Ref 2).

The studies on hot stamping technology of UHSS mainly focus on materials (Ref 3-5), numerical simulation (Ref 6-9) and process modification (Ref 10-13). One of the most important points is phase transformation, which determines the final properties of the hot stamped parts. During the quenching process of hot stamping, the microstructure of the blank is subjected to the transformations from deformed austenite to daughter phases. There is a shift from diffusion phase transformation toward non-diffusion phase transformation with the increase in the cooling rate. Many researchers have studied the diffusion phase transformations of austenite to ferrite, pearlite or bainite during isothermal or non-isothermal deformation. For example, Jin et al. (Ref 14) investigated the effects of isothermal deformation on bainite transformation in alloyed eutectoid steel. It was concluded that the deformed austenite promoted bainite formation by shortening the incubation period and increasing the start temperature of bainite transformation B_s. In 22SiMn2TiB steel studied by Shi et al. (Ref 15), the non-isothermal deformation of austenite was observed to accelerate the diffusion phase transformation. However, for bainite transformation, austenite deformation raised bainite nucleation but retarded bainite growth. Min et al. (Ref 16) reported the phenomenon of ferrite formation induced by the deformation of austenite below A_{e3} and the promotion of bainite transformation below B_s during isothermal deformation in 22MnB5 steel. Further study by Min et al. (Ref 17) showed that when deformed at 923 K, deformation-induced ferrite transformation occurred, and the volume fraction of deformation-induced ferrite increased with an increasing applied strain. When deformed at 693 K, deformation-induced bainite transformation occurred.

Several researchers have focused on the effects of hot deformation on martensitic transformation. Naderi and his fellow researchers investigated the martensitic transformation of 27MnCrB5 boron steel (Ref 18) and 22MnB5 boron steel (Ref 3) by non-isothermal compression tests. The results of both

Yuhan Shen and **Jue Lu**, School of Materials Science and Engineering, Wuhan University of Technology, Wuhan 430070, China; **Yanli Song** and **Lin Hua**, Hubei Key Laboratory of Advanced Technology for Automotive Components, Wuhan University of Technology, Wuhan 430070, China; and Hubei Collaborative Innovation Center for Automotive Components Technology, Wuhan University of Technology, Wuhan 430070, China. Contact e-mail: ylsong@whut.edu.cn.

experiments showed that the start temperature of martensitic transformation (M_s) and the martensite content decreased when applying larger deformation. Abbasi et al. (Ref 19) analyzed the effects of isothermal deformation process variables, namely strain rate and deformation temperature. They reported that the hardness increased with the increase in both strain rate and deformation temperature; the high deformation temperature raised M_s, while strain rate had no significant effect on M_s. The comparison between isothermal and non-isothermal compressions indicated that the former process was characterized by fully martensite as well as lower M_s and M_f over the latter one (Ref 20). Nikravesh et al. (Ref 21) compared the martensitic transformation with and without compressive strains of 0.4. They reported that the martensitic content decreased in a range of cooling rate from 1 to 100 °C/s in deformed condition.

As described above, researches have revealed that the deformation has significant influence on phase transformation. However, most experimental achievements published are limited to the simulated hot stamping process such as uniaxial hot compressive tests or tensile tests. Very few literatures involve the influence and interaction mechanism of plastic deformation on phase transformation during hot stamping of complex structure auto parts. In separate study, the influence of different stress states on martensitic transformation of a hot stamped part in advanced high strength steel (AHSS) was studied by hot stamping experiment (Ref 22). On the one hand, the structures of auto parts are complicated, which means that the amounts of plastic strain are various in different deformation zones. On the other hand, the hot deformation conditions for auto parts are complicated. In a word, part structure and hot deformation condition both affect martensitic transformation and, therefore, influence the homogeneity of the microstructures and properties. Hence, it is important to investigate the martensitic transformation in practical hot stamping process.

In this work, a B-pillar reinforced panel (hereinafter referred to as "Reinf. B-pillar") was selected as a research object. The effects of deformation on martensitic transformation during hot stamping were experimentally studied and theoretically analyzed.

2. Materials and Methods

2.1 Material Properties of B1500HS Steel

The studied material is a cold-rolled boron steel sheet of B1500HS with a thickness of 1.6 mm. The chemical composition (in weight percent) of the boron steel is as follows: C, 0.23; Si, 0.22; Mn, 1.8; P, 0.015; S, 0.001; Cr, 0.16; Ti, 0.04; B, 0.003; N, 0.005. As shown in Fig. 1, the material has a ferritic-pearlitic microstructure in as-delivered condition with yield strength of 330 MPa and tensile strength of 505 MPa or so.

In our previous study, the isothermal tensile tests of B1500HS steel at different temperatures and strain rates were performed on the Gleeble 3500 thermal-simulating machine (Ref 23). Figure 2 shows the stress-strain curves for different temperatures from 600 to 900 °C at strain rates of 0.01, 0.1 and 1/s. The thermo-physical properties are listed in Table 1 (Ref 24).

2.2 Hot Stamping Experiment of Reinf. B-Pillar

The experimental setup for hot stamping is shown in Fig. 3. The hot stamping dies of Reinf. B-pillar were fixed in an electric servo press with a capacity of 600 ton. The transfer system was used for loading of hot blank and unloading of hot formed part.

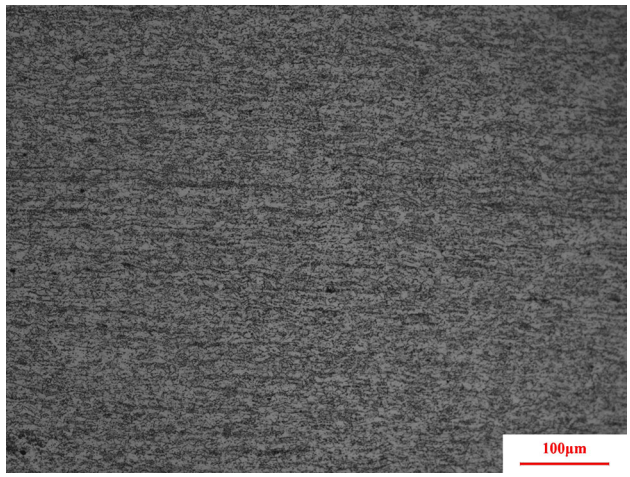

Fig. 1 Microstructure of B1500HS steel in as-delivered condition

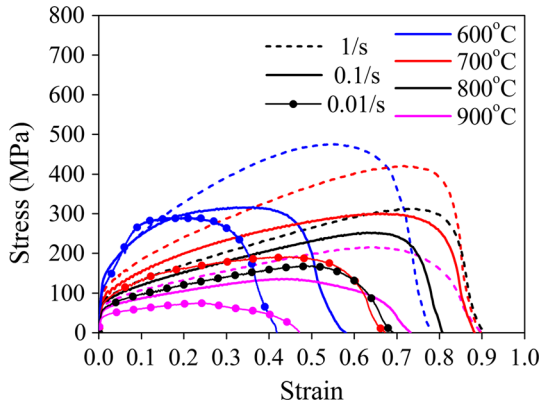

Fig. 2 Flow curves of B1500HS steel at different temperatures and strain rates

During the hot stamping process, the blank of B1500HS steel was initially heated to 930 °C and held for 300 s in the furnace, and then transferred to the press. The hot blank was then formed and subsequently quenched in the water-cooled dies with a holder force of 320 ton. In addition, a pressure-holding time of 10 s was applied during quenching. Finally, the hot stamped part was cooled in the air followed by laser cutting.

2.3 FE Analysis of Reinf. B-Pillar

Based on the FE software AUTOFORM, a thermo-mechanical-metallurgical coupled model was built to simulate the hot stamping process that is heating, transporting, forming, quenching and cooling. The FE model for hot stamping of Reinf. B-pillar is shown in Fig. 4. The simulation parameters are exhibited in Table 2, which are mostly consistent with the experiment parameters.

During the modeling process, the phase transformation is considered and computed based on the chemical composition of B1500HS steel. Since the phase transformation is often accompanied by the change in enthalpy, the latent heat must be taken into account. For martensitic transformation, the value of latent heat is 596 MJ/m^3 when the material is 22MnB5 steel according to the material library of FE software AUTOFORM, which is also used for ferrite, pearlite and bainite.

Table 1 Thermo-physical properties at different temperatures

Temperature, °C	200	300	400	500	600	700	800	900
Specific heat, J/kg K	697	718	697	698	889	1302	1774	1882
Thermal expansion, 10^{-5}/K	2.46	4.05	5.57	7.43	9.03	1.06	9.71	1.12
Heat conductivity, W/m K	42.4	40.5	36.8	34.6	29.5	···	···	···

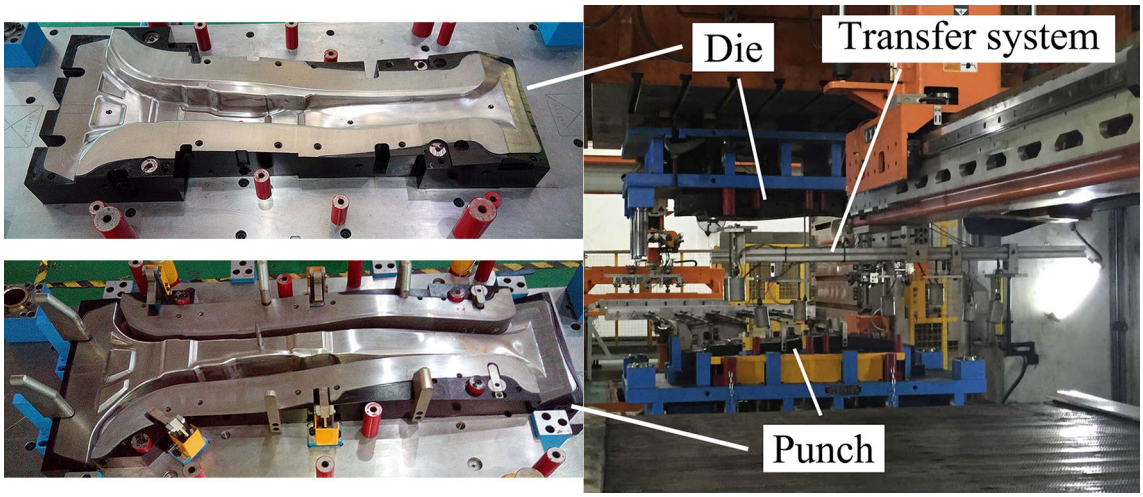

Fig. 3 Experimental setup for hot stamping of Reinf. B-pillar

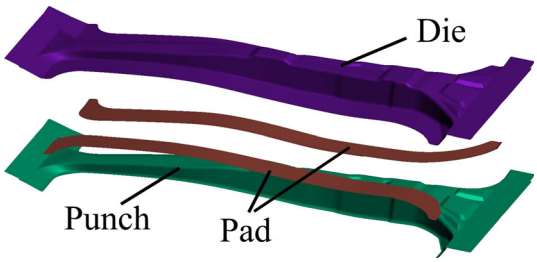

Fig. 4 FE model for hot stamping of Reinf. B-pillar

2.4 Sampling Locations

Figure 5(a) shows the Reinf. B-pillar manufactured by hot stamping experiment. It can be seen that the hot stamped part possesses good formability without splits and wrinkles. Figure 5(b) shows the simulated formability of the hot stamped part. As shown, most areas of the part are sufficiently stretched. No cracking and other defects occur, which is in good agreement with the experimental results.

Figure 6(a) shows the cross-sectional view of the section line A-A in Fig. 5(b). The marked Roman numerals in Fig. 6(a) indicate the sampling locations. The samples cut from the cross section A-A of the hot stamped part are hereinafter called Sample I, Sample II, Sample III and Sample IV. Figure 6(b) shows the equivalent plastic strain contour at the cross section A-A and the strain values at the sampling locations. It is observed that different areas produce different plastic deformation.

The cooling analysis showed that the cooling rates for Sample I, II, III and IV are 157, 167, 157 and 296 °C/s, respectively, at Ms calculated as 386 °C. Therefore, it is reasonable to ignore the influence of cooling rate on martensitic transformation for Sample I, II and III. As for the Sample IV, the influence of cooling rate on martensitic transformation must be considered.

2.5 Validation of the Plastic Deformation Amounts

In order to ensure the effectiveness of sampling, the deformation amounts of the samples were measured by XRD with Cu-Kα radiation in 40 kV voltage and 40 mA current.

Due to the influence of external factors such as machining and thermal cycles, microstrain is produced in the interior of the grains which may broaden the diffraction peaks. Thus, the microstrain is a function of the diffraction line broadening, which can be written as (Ref 25):

$$\varepsilon = \frac{\Delta d}{d} = \frac{\varphi}{4\tan\theta} \quad \text{(Eq 1)}$$

where ε is the microstrain, the ratio between the strain Δd and the interplanar distance d, ϕ is the diffraction line broadening, θ is the diffraction angle.

The microstrain existing in a grain corresponds to the strain on the macroscopic scale. The macro-strain is the equivalent plastic strain calculated by simulation. Figure 7 shows the deformation amounts on macroscopic and microscopic scale. As can be seen from this figure, the variation trend of the simulated equivalent plastic strain is consistent with that of the microstrains measured by XRD. Notably, the numerical comparison has no credibility due to different dimensions.

In the next section, the microstructure morphologies of the samples were observed through scanning electron microscopy (SEM). Also, the microhardness was measured by a microhardness tester with a 300 g load and a dwell time of 5 s. The microhardness test points were in an interval of 0.3 mm. Additionally, more results of XRD analysis were given.

Table 2 Simulation parameters for hot stamping of Reinf. B-pillar

Heating temperature, °C	Transporting time, s	Stamping velocity, mm/s	Friction coefficient	HTC, mW/mm^2 K	Holding pressure, MPa	Holding time, s
930	2	70	0.35	3.5	10	10

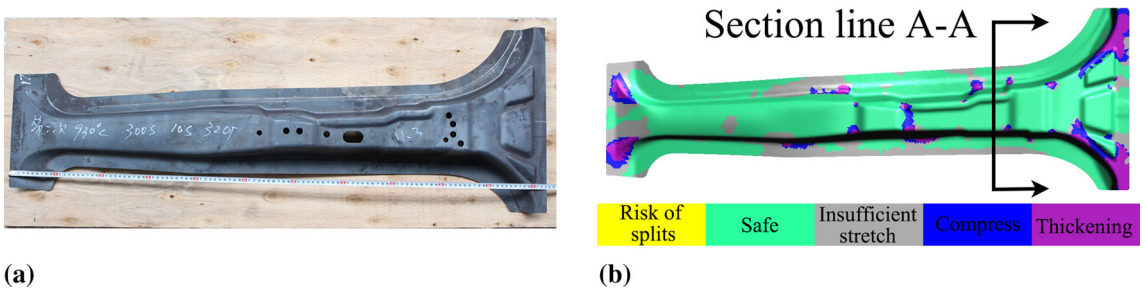

Fig. 5 Hot stamped Reinf. B-pillar: (a) experimental result and (b) simulated result

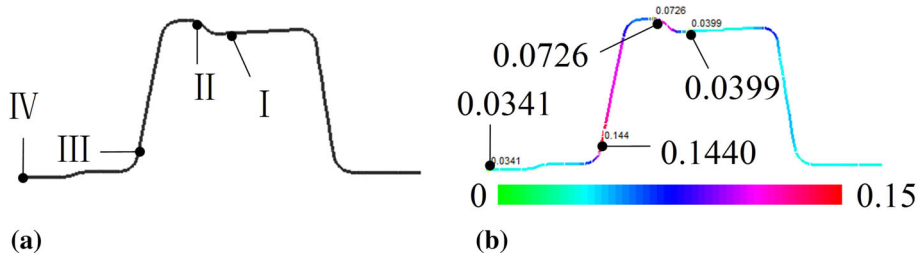

Fig. 6 (a) Cross section A-A and (b) equivalent plastic strain contour at cross section A-A; marked numbers in (a) indicate the sampling locations

3. Results and Discussion

3.1 Effect of Deformation on Martensite During Transformation

Figure 8 shows the microstructure morphologies of four typical samples under SEM. For all the samples studied, martensite is the predominant phase mixed with retained austenite. As can be observed from these figures, Sample III possesses more and finer lath martensite, closely followed by Sample II, then Sample I. It indicates that the martensite content increases with the increase in the deformation amount. Figure 9 shows the microhardness of the samples. It can be found that the microhardness of Sample I, II and III increases progressively in the average values of 458.58, 476.74 and 490.29 HV, respectively. This result coincides well with the conclusion by SEM, since the increased deformation results in higher martensite content and thus higher microhardness.

Similar research results have been reported in some previous literatures. For example, in Fe-0.45C-2.08Si-2.69Mn steel, Shipway and Bhadeshia (Ref 26) analyzed bainite transformation under small stress that less than the yield strength of austenite and demonstrated that the stress possibly accelerates the transformation kinetics.

However, Sample IV is a different case. Although under different applied stress and strain, its microstructure morphology is similar to that of Sample II. Its average microhardness,

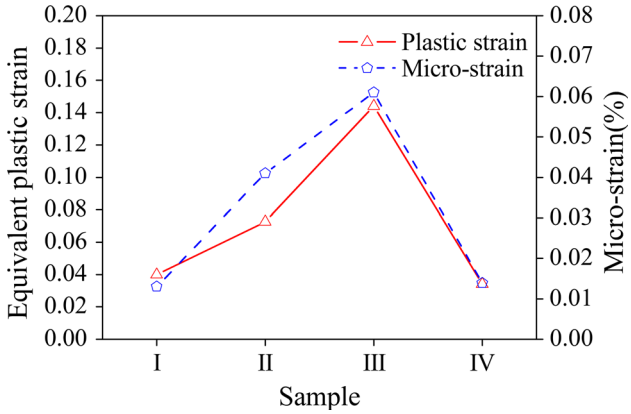

Fig. 7 Deformation amounts of the samples

478.34 HV, is also close to the value of Sample II measured as 476.74 HV. Cooling rate can offer a rational explanation. As mentioned before, Sample IV is taken from the edge of the part where a favorable condition for heat transfer can be provided, and thus the cooling rate of Sample IV is much higher which contributes to martensitic transformation and consequently raises martensite content and the microhardness.

The hot deformation promotes the martensitic transformation in two aspects: On the one hand, the mechanical driving force compensates some driving force for phase transformation;

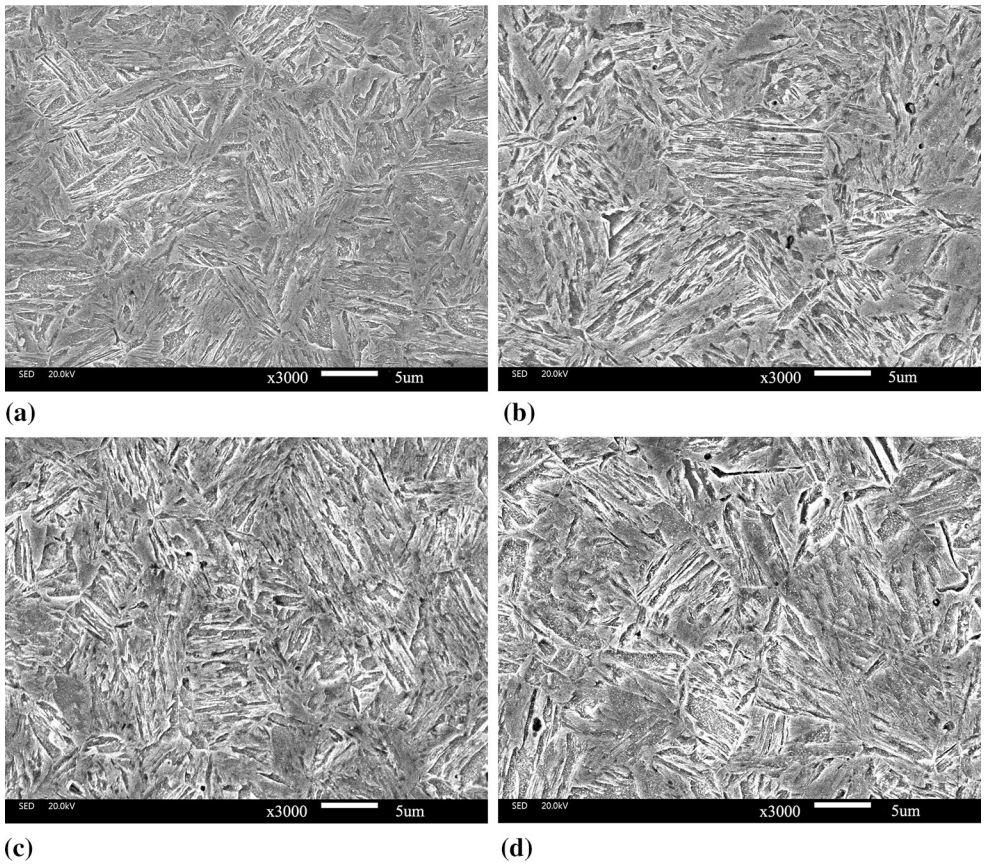

Fig. 8 SEM images of (a) Sample I, (b) Sample II, (c) Sample III and (d) Sample IV

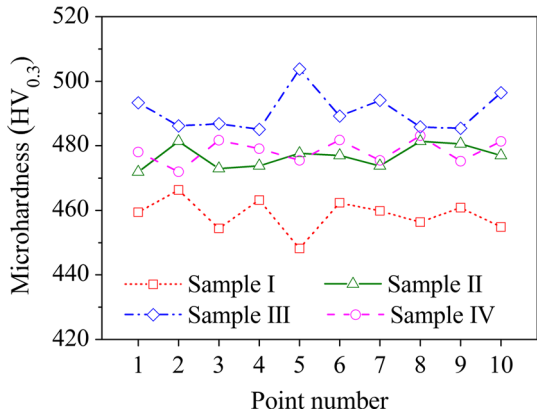

Fig. 9 Microhardness of the samples

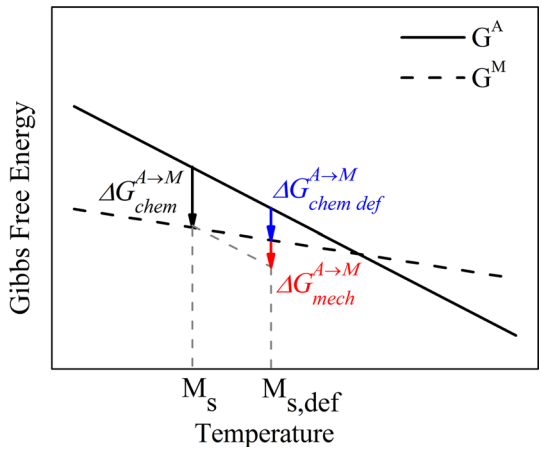

Fig. 10 The schematic of Gibbs free energy change in martensitic transformation

on the other hand, the high density of dislocation makes sites for the nucleation of martensite.

3.1.1 Mechanical Driving Force. Martensitic transformation takes place in a non-diffusion shear type which requires enough driving force to overcome the resistant force including the increased interfacial energy and the increased elastic strain energy resulted from the volume expansion. Figure 10 shows the change of Gibbs free energy during martensitic transformation (Ref 19). In non-deformed condition, the driving force is the difference of Gibbs free energy between austenite and martensite, called chemical driving force (expressed as $\Delta G_{\text{chem}}^{A\rightarrow M}$). Generally, the chemical driving force is achieved by undercooling. As illustrated in Fig. 10, the chemical driving force increases as the temperature decreases. In deformed condition, the strain energy generated by plastic deformation serves as mechanical driving force (expressed as $\Delta G_{\text{mech}}^{A\rightarrow M}$) and thus less chemical driving force is demanded for martensitic transformation, which brings about a raise of martensite start temperature from M_s to $M_{s,\text{def}}$.

According to the criterion for the effect of applied stress on martensitic transformation proposed by Patel and Cohen (Ref 27), the mechanical driving force includes two terms: the work

from the shear stress and the work from the normal stress, as shown in Eq 2.

$$U = \tau\gamma_0 + \sigma\varepsilon_0 \quad \text{(Eq 2)}$$

where U is the work done by the applied stress, τ is the shear stress, γ_0 is the shear strain, σ is the normal stress (positive when the normal stress is tensile, and negative when this component is compressive) and ε_0 is the normal strain.

Assuming that the blank is in plane stress condition during hot stamping, the shear stress and normal stress can be exhibited by Mohr's circle in Fig. 11. Thus,

$$\begin{cases} \tau = \frac{\sigma_1-\sigma_2}{2}\sin 2\theta' \\ \sigma = \frac{\sigma_1+\sigma_2}{2} + \frac{\sigma_1-\sigma_2}{2}\cos 2\theta' \end{cases} \quad \text{(Eq 3)}$$

where σ_1 is the major stress, σ_2 is the minor stress and θ' is the angle between the physical plane and the normal to the habit plane. In a similar way, the shear strain and normal strain can be calculated by

$$\begin{cases} \gamma_0 = \frac{\varepsilon_1-\varepsilon_2}{2}\sin 2\theta' \\ \varepsilon_0 = \frac{\varepsilon_1+\varepsilon_2}{2} + \frac{\varepsilon_1-\varepsilon_2}{2}\cos 2\theta' \end{cases} \quad \text{(Eq 4)}$$

where ε_1 is the major strain, ε_2 is the minor strain. Therefore, U may now be expressed as a function of principal strains and principal stresses:

$$U = \frac{\sigma_1-\sigma_2}{2}\frac{\varepsilon_1-\varepsilon_2}{2} + \frac{\sigma_1+\sigma_2}{2}\frac{\varepsilon_1+\varepsilon_2}{2} + \left(\frac{\sigma_1-\sigma_2}{2}\frac{\varepsilon_1+\varepsilon_2}{2} + \frac{\sigma_1+\sigma_2}{2}\frac{\varepsilon_1-\varepsilon_2}{2}\right)\cos 2\theta' \quad \text{(Eq 5)}$$

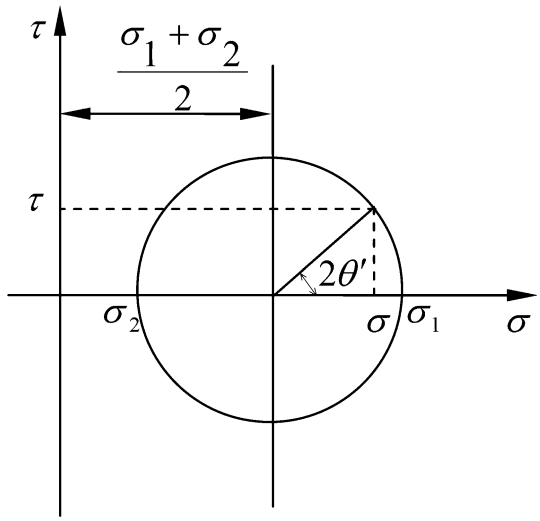

Fig. 11 Mohr's circle in plane stress condition

It is assumed that U_{max} contributes to the Gibbs free energy change, and

$$\Delta G_{mech}^{A\to M} = U_{max} = \sigma_1\varepsilon_1 \quad \text{(Eq 6)}$$

Substituting the simulated major strains and major stresses into Eq 6, it is now possible to obtain the values of U_{max}.

Table 3 lists the simulated principal strains, principal stresses and calculated mechanical driving forces at four sampling locations. As can be seen from this table, the strain values match with the stress magnitudes. Moreover, the stress states of all the samples are tension dominant, which stimulates the phase transformation according to Eq 2. When adding the applied major stress from 198 to 300 MPa, the mechanical driving force can be raised by 220 J/mol. Consequently, martensitic transformation is induced above M_s by plastic deformation and martensite start temperature increases with the increase in stress or strain.

3.1.2 Martensitic Nucleation. Regardless of composition change, the occurrence of martensitic transformation depends not only on energy but also on structure. The crystal defects can provide the necessary structure and energy fluctuations for martensitic nucleation. The structure-energy feedbacks magnify fluctuation and thus causing the instability of austenitic structure and establishment of martensitic structure. When martensites nucleate at the dislocations in the austenite grains, the change of system Gibbs free energy caused by nucleation can be defined as (Ref 28):

$$\Delta G = V\Delta g + VU_V + A\psi - he \quad \text{(Eq 7)}$$

where Δg is the driving force for martensitic transformation, U_V is the strain energy, ψ is the interface energy, e is the dislocation strain energy, V is the nuclear volume, A is the surface area and h is the nuclear length. The second and the third terms are the phase transformation resistant force; the fourth term is the contribution of the dislocation to nucleation. In deformed condition, a lot of crystal defects such as point dislocations and line dislocations are introduced into the grain interiors and the grain boundaries. According to Eq 7, dislocations contribute to making preferred nucleation sites for martensitic transformation by reducing ΔG.

Hsu (Ref 29) quantitatively described the effects of stress and strain on nucleation barrier that the nucleation barrier is inversely proportional to the function of stress and strain. Therefore, adding the applied stress or strain helps to decrease the nucleation barrier and thus increases the nucleation rate. Besides, the plastic deformation induces the grain breaking of austenite, leading to the grain refinement of martensite.

During the hot stamping process, the stress concentration is inclined to generate at the grain boundaries, providing energy for priority martensitic nucleation in the grain boundaries. Figure 12(a) presents the SEM image of martensitic nucleation in the grain boundary. As can be seen in this figure, the lath martensite nucleates in the grain boundary and propagates into

Table 3 Simulated principal strains, principal stresses and calculated mechanical driving forces of four samples

Sample	Major strain	Minor strain	Major stress, MPa	Minor stress, MPa	U_{max}, J/mol
I	0.0294	0.00813	198	169	41
II	0.0381	0.00688	235	210	63
III	0.1230	−0.04940	300	263	261
IV	0.0147	0.00124	179	175	19

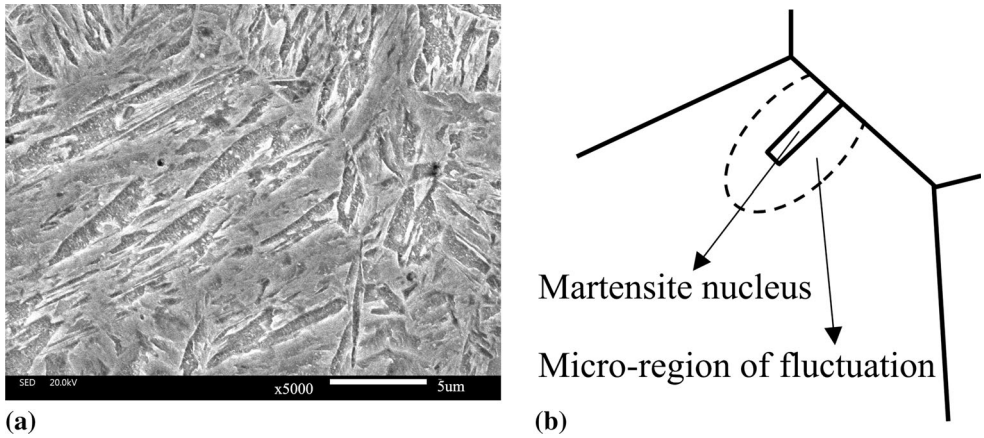

Fig. 12 (a) SEM image of Sample II and (b) the schematic of martensitic nucleation in the grain boundary

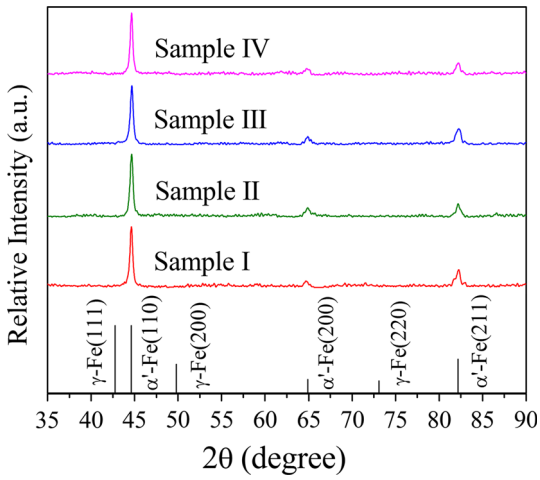

Fig. 13 XRD patterns of the samples

the grain. Figure 12(b) shows a schematic of martensitic nucleation. The microregion of fluctuation provides thermodynamic conditions for martensitic nucleation. Based on the crystal defect and assisted by the defect energy, the martensite nucleus is formed.

3.2 Effect of Deformation on Retained Austenite During Transformation

Figure 13 presents the XRD patterns of all samples in comparison with the standard patterns of martensite and austenite. It can be observed that the XRD patterns feature three distinct diffraction peaks. Take the pattern of Sample III for instance. The high-intensity peak corresponding to the (110) is positioned at 44.677° with an interplanar distance d = 0.20266 nm, which is basically coincident with the standard peak position of 44.622° for martensite in (110). The measured and the standard peak position for austenite in (111) are 42.678° and 42.758°, respectively, with a difference value of 0.040°, which means that the measured diffraction peak line moves to the left. Extensive studies on phase transformation have revealed that certain orientation relationship exists between the new phase and the parent phase. The orientation relationship between martensite and austenite can be obtained by the application of XRD. The difference between the measured peak positions for martensite and austenite is 0.9995° which conforms to the *K-S* orientation relationship.

The lattice parameter and carbon content of retained austenite can be calculated through XRD. Austenite has the face-centered cubic structure, in which:

$$a = b = c, \quad \alpha = \beta = \gamma = 90^\circ \tag{Eq 8}$$

where $a, b, c, \alpha, \beta, \gamma$ are lattice parameters. The lattice parameter a can be calculated based on the peak position as follows (Ref 25):

$$a = \frac{\lambda}{2\sin\theta}\sqrt{h^2 + k^2 + l^2} \tag{Eq 9}$$

and according to Bragg equation

$$d = \frac{\lambda}{2\sin\theta} \tag{Eq 10}$$

where λ is the wave length of x-ray, θ is the diffraction angle, (hkl) are indices of crystal face and d is the interplanar distance.

For most of the solid solution, the lattice parameter increases with the increase in the solute concentration and their relation is approximately linear, obeying Vegard's law. The carbon content of austenite can be estimated by using the following equation (Ref 30):

$$a = 0.3573 + 0.033 \times (\text{wt.\%C}) \tag{Eq 11}$$

Figure 14 shows the lattice parameters and carbon contents of retained austenite in the samples. As shown in the figure, for all samples, the carbon contents of retained austenite exceed the value of 0.23% in B1500HS steel. Barnard et al. (Ref 31) observed the carbon diffusion to enrich the retained austenite films which provided direct evidence of the chemical stabilization of this phase. Additionally, Hsu et al. (Ref 32) calculated the time required for carbon enrichment in retained austenite during the formation of low-carbon martensite. They pointed out that carbon diffusion may occur concomitantly with the formation of lath martensite and keep pace with or slightly lag behind it. They further supposed that the diffusion of carbon atoms is not a primary process in martensitic transformation, for that the diffusion of interstitial atom carbon has no impact on the diffusionless displacement of the replace atoms. However, the carbon enrichment of the retained austenite can help enhance the stability.

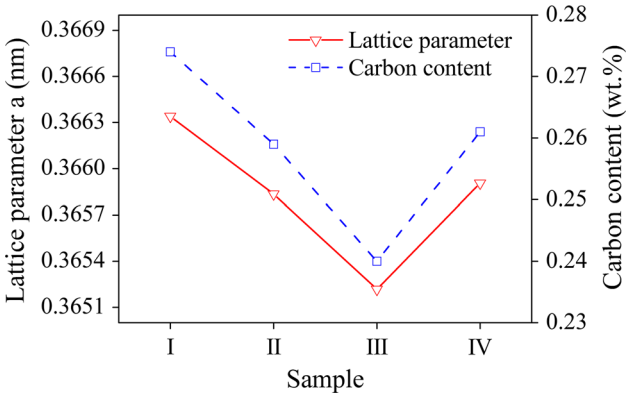

Fig. 14 Lattice parameters and carbon contents in γ-Fe of the samples

On the other hand, the carbon levels in the austenite phase are further found to change over the deformation amounts as shown in Fig. 14. It is reasonable to conclude that the deformation affects the processing of carbon diffusion. It is known that the segregation of carbon is produced at the dislocation sites during the formation of low-carbon martensite. This may prolong the diffusion time and consequently reduce the diffusion coefficient. Therefore, the diffusion of carbon atom is retarded by deformation. Besides, the high cooling rate seems to retard the carbon diffusion too. This phenomenon also happens in the case of diffusion phase transformation. The study of ferrite transformation by Shi et al. (Ref 33) reported that the content of retained austenite decreases with decreasing carbon content as the deformation amount increases. They suggested that the deformation of austenite leads to the changes of lattice parameters due to carbon partition and elastic strain during the transformation.

4. Conclusions

In the current work, the effects of deformation amount on martensitic transformation of B1500HS steel after hot stamping of a Reinf. B-pillar were investigated by using the combined method of simulations and experiments. It is concluded that:

1. With the increase in plastic strain, the martensitic content increases and the grains are refined, leading to a higher microhardness value. Despite of small plastic deformation, a high cooling rate contributes to martensitic transformation.
2. Deformation stimulates martensitic transformation by lowering the chemical driving force. When adding the applied major stress from 198 to 300 MPa, the mechanical driving force can be raised from 41 to 261 J/mol. Deformation also increases the probability of the martensitic nucleation at dislocations and the grain boundaries.
3. Carbon is enriched in retained austenite during low-carbon martensitic transformation. Deformation of austenite can suppress the carbon diffusion. Thus, as the deformation amount increases, the carbon content decreases.

Acknowledgments

This work was supported by the National Natural Science Foundation of China (Grant Nos. 51305317 and 51675392); China Automobile Industry Innovation and Development Joint Fund (Grant No. U1564202); and the Special Foundation of Technological Innovation of Hubei Province (Grant No. 2016AAA053).

References

1. H. Karbasian and A.E. Tekkaya, A Review on Hot Stamping, *J. Mater. Process. Technol.*, 2010, **210**(15), p 2103–2118
2. M. Merklein and J. Lechler, Investigation of the Thermo-Mechanical Properties of Hot Stamping Steels, *J. Mater. Process. Technol.*, 2006, **177**(1-3), p 452–455
3. M. Naderi, L. Durrenberger, A. Molinari, and W. Bleck, Constitutive Relationships for 22MnB5 Boron Steel Deformed Isothermally at High Temperatures, *Mater. Sci. Eng. A*, 2008, **478**(1-2), p 130–139
4. M. Abspoel, B.M. Neelis, and P.V. Liempt, Constitutive Behaviour Under Hot Stamping Conditions, *J. Mater. Process. Technol.*, 2016, **228**, p 34–42
5. H.P. Li, L.F. He, G.Q. Zhao, and L. Zhang, Constitutive Relationships of Hot Stamping Boron Steel B1500HS Based on the MODIFIED ARRHENIUS and Johnson-Cook Model, *Mater. Sci. Eng. A*, 2013, **580**, p 330–348
6. H.H. Bok, M.G. Lee, H.D. Kim, and M.B. Moon, Thermo-mechanical Finite Element Analysis Incorporating the Temperature Dependent Stress–Strain Response of Low Alloy Steel for Practical Application to the Hot Stamped Part, *Met. Mater. Int.*, 2010, **16**(2), p 185–195
7. H.H. Bok, M.G. Lee, E.J. Pavlina, F. Barlat, and H.D. Kim, Comparative Study of the Prediction of Microstructure and Mechanical Properties for a Hot-Stamped B-Pillar Reinforcing Part, *Int. J. Mech. Sci.*, 2011, **53**(9), p 744–752
8. H.H. Bok, J.W. Choi, F. Barlat, D.W. Suh, and M.G. Lee, Thermo-mechanical–Metallurgical Modeling for Hot-Press Forming in Consideration of the Prior Austenite Deformation Effect, *Int. J. Plast.*, 2014, **58**(1), p 154–183
9. P. Hippchen, A. Lipp, H. Grass, P. Craighero, M. Fleischer, and M. Merklein, Modelling Kinetics of Phase Transformation for the Indirect Hot Stamping Process to Focus on Car Body Parts with Tailored Properties, *J. Mater. Process. Technol.*, 2016, **228**, p 59–67
10. R. Kolleck, R. Veit, M. Merklein, J. Lechler, and M. Geiger, Investigation on Induction Heating for Hot Stamping of Boron Alloyed Steels, *CIRP Ann. Manuf. Technol.*, 2009, **58**(1), p 275–278
11. H.S. Choi, B.M. Kim, K.J. Nam, S.Y. Ha, S.H. Cha, and C.G. Kang, Development of Hot Stamped Center Pillar Using Form Die with Channel Type Indirect Blank Holder, *Int. J. Automot. Technol.*, 2011, **12**(6), p 887–894
12. M. Naderi, M. Ketabchi, M. Abbasi, and W. Bleck, Analysis of Microstructure and Mechanical Properties of Different High Strength Carbon Steels After Hot Stamping, *J. Mater. Process. Technol.*, 2011, **211**(6), p 1117–1125
13. W.S. Lim, H.S. Choi, S.Y. Ahn, and B.M. Kim, Cooling Channel Design of Hot Stamping Tools for Uniform High-Strength Components in Hot Stamping Process, *Int. J. Adv. Manuf. Technol.*, 2014, **70**(5-8), p 1189–1203
14. X.J. Jin, N. Min, K.Y. Zheng, and T.Y. Hsu, The Effect of Austenite Deformation on Bainite Formation in an Alloyed Eutectoid Steel, *Mater. Sci. Eng. A*, 2006, **438-440**, p 170–172
15. Z. Shi, K. Liu, M. Wang, J. Shi, H. Dong, J. Pu, B. Chi, Y. Zhang, and L. Jian, Effect of Non-isothermal Deformation of Austenite on Phase Transformation and Microstructure of 22SiMn2TiB Steel, *Mater. Sci. Eng. A*, 2012, **535**(4), p 290–296
16. J. Min, J. Lin, Y. Min, and F. Li, On the Ferrite and Bainite Transformation in Isothermally Deformed 22MnB5 Steels, *Mater. Sci. Eng. A*, 2012, **550**(31), p 375–387
17. J. Min, J. Lin, and Y. Min, Effect of Thermo-mechanical Process on the Microstructure and Secondary-Deformation Behavior of 22MnB5 Steels, *J. Mater. Process. Technol.*, 2013, **213**(6), p 818–825
18. M. Naderi and W. Bleck, Martensitic Transformation During Simultaneous High Temperature Forming and Cooling Experiments, *Steel Res. Int.*, 2007, **78**(12), p 914–920
19. M. Abbasi, A. Saeed-Akbari, and M. Naderi, The Effect of Strain Rate and Deformation Temperature on the Characteristics of Isothermally Hot Compressed Boron-Alloyed Steel, *Mater. Sci. Eng. A*, 2012, **538**, p 356–363

20. M. Abbasi, M. Naderi, and A. Saeed-Akbari, Isothermal Versus Non-isothermal Hot Compression Process: A Comparative Study on Phase Transformations and Structure–Property Relationships, *Mater. Des.*, 2013, **45**, p 1–5
21. M. Nikravesh, M. Naderi, G.H. Akbari, and W. Bleck, Phase Transformations in a Simulated Hot Stamping Process of the Boron Bearing Steel, *Mater. Des.*, 2015, **84**, p 18–24
22. Y. Chang, X.D. Li, K.M. Zhao, C.Y. Wang, G.J. Zheng, P. Hu, and H. Dong, Influence of Stress on Martensitic Transformation and Mechanical Properties of Hot Stamped AHSS Parts, *Mater. Sci. Eng. A*, 2015, **629**, p 1–7
23. J.N. Liu, Y.L. Song, J. Lu, and W. Guo, Effect Laws and Mechanisms of Different Temperatures on Isothermal Tensile Fracture Morphologies of High-Strength Boron Steel, *J. Cent. South Univ.*, 2015, **22**(4), p 1191–1202
24. J.N. Liu, Study on Deformation Behaviour and Microstructure and Properties of Hot Stamping of UHSS B-Pillar, Master thesis, Wuhan University of Technology, China, p 14–17, 2015 (**in Chinese**)
25. J.W. Huang and Z. Li, *X-Ray Diffraction of Polycrystalline Materials*, Metallurgical Industry Press, Beijing, 2012, p 159–161 (**in Chinese**)
26. P.H. Shipway and H.K.D.H. Bhadeshia, The Effect of Small Stresses on the Kinetics of the Bainite Transformation, *Mater. Sci. Eng. A*, 1995, **201**(1-2), p 143–149
27. J.R. Patel and M. Cohen, Criterion for the Action of Applied Stress in the Martensitic Transformation, *Acta Metall.*, 1953, **1**(5), p 531–538
28. G.B. Olson and M. Cohen, A Perspective on Martensitic Nucleation, *Annu. Rev. Mater. Sci.*, 2003, **11**(1), p 1–32
29. T.Y. Hsu, Martensitic Transformation Under Stress, *Mater. Sci. Eng. A*, 2006, **438-440**, p 64–68
30. N. Ridley, H. Stuart, and L. Zwell, Lattice Parameters of Fe-C Austenites at Room Temperature, *Trans. Metall. Soc. AIME*, 1969, **245**(8), p 1834–1836
31. S.J. Barnard, G.D.W. Smith, M. Sarikaya, and G. Thomas, Carbon Atom Distribution in a Dual Phase Steel: An Atom Probe Study, *Scripta Metall.*, 1981, **15**(4), p 387–392
32. T.Y. Hsu and X. Li, Diffusion of Carbon During the Formation of Low-Carbon Martensite, *Scripta Metall.*, 1983, **17**(11), p 1285–1288
33. Z. Shi, Y. Tomota, S. Harjo, Y. Su, B. Chi, J. Pu, and L. Jian, Effect of Non-isothermal Deformation of Austenite on Ferrite Transformation Behavior Studied by In Situ Neutron Diffraction, *Mater. Sci. Eng. A*, 2015, **631**, p 153–159